K^-K^+ and $\pi^-\pi^+$ Production in K^-p Interactions at 13 GeV*

by

G.W. Brandenburg

Laboratory for Nuclear Science,

Massachusetts Institute of Technology, Cambridge, Mass. 02139

* Work supported by U.S. Energy Research and Development Administration

Talk presented at the Summer Symposium on New Directions in Hadron Spectroscopy, Argonne National Laboratory, July, 1975.

Conf-750749--2

COO-3069-46

OSP-72

1.0 Introduction

The production of dipion and dikaon states with a K^- beam is interesting in several respects. For example all three vector mesons are produced with comparable hypercharge exchange amplitudes in these reactions. This is to be contrasted with π-induced reactions where there is little ϕ production and where g-parity demands different exchanges for ρ^0 and ω production. In addition to the ϕ, the production of other $\bar{K}K$ states such as the S* and f' is also enhanced since an incident $\bar{K}K$ state is obtained via K exchange.

Vector meson production with hypercharge exchange has been studied at lower energies where it was also possible to measure the polarization of the recoiling Λ or Σ^0.[1,2,3] In a high-statistics spark chamber experiment performed by SLAC Group B, these measurements have been extended to high energies.[4] Since the recoil baryon is inferred from the missing mass in our experiment, we do not measure the Λ or Σ^0 polarization. However, our increased sensitivity makes it possible to study other subtle effects such as ρ^0-ω interference and S* production.

A brief description of the experiment follows in Section 2. The production of ϕ and ρ^0 mesons is analyzed and discussed in Section 3. The phenomenon of ρ^0-ω interference is the subject of Section 4. Finally, the observation of S* production is presented in Section 5.

2.0 The Experiment

The experiment was performed in an RF separated 13 GeV K^- beam at SLAC using a wire spark chamber spectrometer system.[5] Fig. 1 shows a plan view of the apparatus. Scintillation counter hodoscopes, two threshold Cerenkov counters, and 1 mm wire spacing proportional

DISCLAIMER

chambers ___ used to measure the mass, momentum, and trajectory of each beam particle incident on the 1 meter long hydrogen target. The beam resolutions are ± 0.3% in momentum, ± 0.5 mrad in angle, and ± 1 mm in space at the interaction point. The dipole magnet aperture is 0.6 m high x 1.8 m wide and has a field integral of 18 kg m. The nine magnetostrictive readout wire spark chambers each consist of 2 gaps with 4 readout coordinates and have small polyurethane plugs installed through which the beam passes. The spark chamber lever arms are 1 m upstream and 2 m downstream of the magnet, yielding secondary momentum resolution better than 1%. The observed 13 GeV $K^o \to \pi^+\pi^-$ decay invariant mass distribution has a FWHM = 12 MeV.

The trigger for the experiment, defined using several scintillation counter hodoscopes, required that 2 or more charged particles pass through the spectrometer after originating from an interaction in the hydrogen target. In addition, the magnet was lined with scintillation counters to reject events in which a secondary particle strikes the pole piece. The large aperture Cerenkov counter contained eight optically distinct elements and provided K, π identification of the secondary particles.[6]

3.0 ϕ and ρ^0 Meson Production

The production of vector mesons recoiling against Λ or Σ^0 hyperons is a prominent feature of both the K^-K^+ and $\pi^-\pi^+$ channels. These reactions involve hypercharge exchange in the t-channel and thus are a good source of information on K* and K exchange. In this section, we analyze the production and decay distributions of the ϕ and ρ^0 mesons and discuss the general characteristics of the data.

3.1 Data Selection

The large threshold Cerenkov counter described in Section 2 is used to identify the K^-K^+ and $\pi^-\pi^+$ data. In both cases the dominant background is from the reaction $K^-p \to K^-\pi^+(MM)$. Therefore the $\pi^-\pi^+$ events are selected by requiring that the negative particle be a π^-. This leaves a small contamination from K^- decays, which can easily be estimated using the measured $K^-\pi^+$ events. The strong ϕ signal, on the other hand, allows a weaker selection criterion to be used for K^-K^+ events in the ϕ region. In particular we require that any positive particle entering the Cerenkov counter not be a π^+; if a particle misses the counter it is assumed to be a K^+. The resulting $K^-\pi^+$ contamination of the ϕ data is less than 2%.

The recoil missing mass spectra for events in the ϕ ($1.009 < M(\bar{K}K) < 1.029$ GeV) and the ρ^0 ($0.70 < M(\pi\pi) < 0.84$ GeV) regions are shown in Figs. 2a and 2b respectively. In both distributions there is a broad peak encompassing both the Λ and Σ^0 hyperons, followed by a substantial dip at 1.3 GeV. Our experimental missing mass resolution is not sufficient to resolve the Λ and Σ^0 peaks, but it provides adequate separation from higher mass hyperon states. There is also a strong peak at the Λ(1520) in Fig. 2, and some evidence for Y*(1385) production. For the study of the $\phi(\Lambda, \Sigma^0)$ final state we select the events in the interval $1.00 < MM < 1.25$ GeV. For the $\rho^0(\Lambda, \Sigma^0)$ final state, the contaminating $K^-\pi^+n$ events peak at a missing mass of 0.97 GeV; therefore we use a tighter cut, $1.05 < MM < 1.225$ GeV.

The K^-K^+ mass spectrum for the selected $K^-K^+(\Lambda, \Sigma^0)$ events is shown in Fig. 3a. In order to display the full mass range, only those

events with a positively identified K^+ have been plotted here. The histogram has not been corrected for the experimental acceptance, which decreases smoothly with increasing mass. In the high mass region there is a large peak at the f'(1514). The decay of the f' is discussed in a forthcoming publication.[4] The ϕ peak appears to have a broad shoulder in Fig. 3a; however, when replotted on a finer scale in Fig. 3b, the ϕ is cleanly separated from a structure at 1.07 GeV. This shoulder is the result of the K*(890) decay into a K^- and a π^+ which has been misidentified as a K^+. The less stringent requirement that the positive particle not be identified as a π^+ was used in plotting Fig. 3b and, as was discussed above, the resulting ϕ peak has less than 2% $K^-\pi^+$ contamination. For further study the reaction $K^-p \to \phi(\Lambda, \Sigma^0)$ is selected by the mass cut $1.009 < M(\bar{K}K) < 1.029$ GeV.

The $\pi^-\pi^+$ mass spectrum is shown for events recoiling against a (Λ, Σ^0) mass in Fig. 4. The sharp peak at the K^0 mass is from $K^-p \to \bar{K}^0(n,\Delta^0)$ events where the missing mass has fallen in the (Λ,Σ^0) cut. Above the ρ^0 peak there is evidence for S* production at 0.98 GeV (see Section 5) and a broad peaking at the $f^0(1270)$. As in Fig. 3, the histogram is uncorrected for the smoothly varying acceptance. The dotted curve under the ρ^0 is the estimated $K^-\pi^+$ contamination; the K*(890) decay causes this contamination to peak below 0.7 GeV. The actual $\pi^-\pi^+$ background under the ρ^0 does not appear to be very large; in fact the data are consistent with being pure P-wave in this region (see Section 3.3). The $\pi^-\pi^+$ mass cut $0.7 < m_{\pi\pi} < 0.84$ GeV is used to define the $K^-p \to \rho^0(\Lambda,\Sigma^0)$ data sample.

3.2 Angular Distribution Analysis

We have extracted the spherical harmonic moments $\langle Y_{\ell m}\rangle$ of both

the ϕ and ρ^0 decay angular distributions as functions of $t' = -t + t_{min}$. The technique used was to perform a maximum likelihood fit of the data to an acceptance corrected sum of spherical harmonies, $Y_{\ell m}$. Fits were done in both the s-channel and the t-channel (Gottfried-Jackson) helicity systems with a maximum ℓ of two. In the case of the ρ^0 it was necessary to weight the data on an event by event basis to correct for the $K^-\pi^+$ contamination. In addition to the moments, the fits also yield the corrected number of events in a given t' bin. Multiplying by the experiment normalization factor,[4] we then obtain an acceptance corrected differential cross section .

In Figs. 5 and 6 the solid points show corrected differential cross sections versus t' for the ϕ and ρ^0. The ϕ cross section has a dip at $t' = 0$ and falls off exponentially above $t' = 0.1$ GeV^2 with a slope of approximately 3 GeV^{-2} . The ρ^0 data, though somewhat sparse, are similar in shape and magnitude to the $\phi \to K^-K^+$ cross section.

3.3 S-Wave Background

As noted above, for both the ϕ and ρ^0, the actual nonresonant background is consistent with being zero. When the small $K^-\pi^+$ contamination is subtracted from Fig. 3a, the ϕ shape can be accounted for by the experimental mass resolution and no additional background. In the following section it is demonstrated that a fit to the ρ^0 peak also requires no background, although an interfering ω is required.

These observations are augmented by the fact that the values of the density matrix elements $Re\rho_{0_S}$ and $Re\ \rho_{1S}$ are consistent with zero for all t'. This means that any S-wave background is either incoherent or 90° out of phase with the P-wave resonances. The latter

possibility was ruled out by measuring the values of Re ρ_{ms} for the upper and lower sides of the resonance peaks; they were again found to be zero. Therefore although a small incoherent S-wave background cannot be ruled out, we will assume the ϕ and ρ^0 mass regions are pure P-wave.

This is not surprising in the case of the ρ^0. Although there is a broad S-wave enhancement under the pion produced ρ^0,[7] the so-called ε, this dipion state is coupled to a $\pi\pi$ initial state. In the reaction under study the ε would have to couple to a $\bar{K}K$ initial state, considerably below $\bar{K}K$ threshold. Any S-wave that was produced underneath the ρ^0 would add incoherently, however, since an S-wave $\pi\pi$ system must be produced by unnatural parity exchange and the ρ^0 is produced predominantly natural parity exchange as discussed below.

The possibility of observing the S-wave S* resonance at K^-K^+ threshold does exist, but the effect is overwhelmed by the neighboring ϕ peak. The S* in the $\pi^-\pi^+$ channel is the subject of Section 5.

3.4 Natural and Unnatural Parity Exchange

Having assumed that the background to vector meson production is nonexistant, i.e., $\rho_{ss} = 0$, it is possible to obtain the elements ρ_{00} and ρ_{11}. In addition the ρ^0 decay distributions were unanalyzed assuming both $\ell = 1$ moments (i.e.Re ρ_{0s} and Re ρ_{1s}) were zero for more accurate determinations of the P-wave density matrix elements. We then form the combinations $\rho_{\pm} = \rho_{11} \pm \rho_{1-1}$, which to a good approximation at our energy project the natural (ρ_+) and unnatural (ρ_-) parity exchange components to helicity one vector meson production.[8] The helicity zero state (ρ_{00}) can only be produced by

unnatural parity exchange. Multiplying the differential cross section $d\sigma/dt'$ by ρ_+, ρ_-, and ρ_{00} gives the cross section for production in each helicity and exchange parity state: σ_+, σ_-, and σ_0. The cross sections thus obtained are plotted in Figs. 5 and 6 together with the total differential cross section. σ_+ is invariant under rotations between the s-and t-channel frames, whereas σ_- and σ_0 are not.

It is immediately clear from Figs. 5 and 6 that ϕ and ρ^0 mesons are produced dominantly by natural parity exchange in the reactions being studied. For the ϕ, σ_+ is approximately 80% of $d\sigma/dt'$ for all values of t'; in the case of the ρ^0 the fraction is about 60%. The leading trajectories for natural parity exchange are the K* and K**.

Because of the dip at $t' = 0$ in Figs. 5 and 6, the dominant contribution to σ_+ appears to be a helicity flip amplitude. The natural parity exchange amplitude must be flip at the meson vertex; if in addition it is non-flip at the baryon vertex there must be such a dip. On the other hand, if the baryon vertex also has a unit helicity flip, then the total helicity flip can be zero and absorption is expected to fill in the forward dip.[9] To obtain a rough estimate of the fraction of σ_+ which has a net helicity flip of one, we have fit the ϕ data for $t' < 0.5$ GeV^2 to the functional form $c(a + t')\, e^{-bt'}$. The purely exponential term represents the contribution with zero net helicity flip. Integrating the resulting expression over t' we find the fraction of σ_+ with a net helicity flip to be 86 ± 5%. We also note that the four ρ^0 points for σ_+ are consistent with this fit.

We now turn to the smaller unnatural parity exchange cross sections for the ϕ meson. In the s-channel, σ_0 has a forward peak and

then falls to zero at $t' \sim 0.4$ GeV^2. On the other hand σ_- has a shape similar to σ_+ for $t' \gtrsim 0.4$ GeV^2, but is about 25% as large. σ_0 and σ_- in the t-channel are similar in behavior for small t', but for $t' \gtrsim 0.4$ GeV^2 they reverse with σ_0 remaining large. This can be understood by considering the s-t crossing angle; it is 180° at $t' = 0$, but falls quickly to ∿100° by $t' = 0.4$ GeV^2. For larger t' the crossing angle stays near 90°, which simply interchanges σ_0 and σ_-.

The unnatural parity exchange cross sections for ρ^0 production resemble those for the ϕ, but with the roles of σ_0 and σ_- reversed. In the t-channel it is σ which remains a constant fraction (∿40%) of σ_+, while σ_0 drops off sharply. As with the ϕ, the crossing angle is ∿90° for $t' > 0.2$ GeV^2, so the behavior of σ_0 and σ_- in the s-channel (not shown) is again just the reverse of that shown in Fig. 6 for the t-channel.

Absorption of the dominant natural parity exchange amplitude could result in some feedthrough into the unnatural parity ones. However, it is well known that such feedthrough should only affect σ_- and not σ_0.[9] Furthermore, because σ_+ is predominantly helicity flip, it is not expected to be strongly absorbed. Therefore we conclude that σ_0 and σ_- do indeed represent unnatural parity exchange in the reactions studied. We note that ρ_+ has risen from ∿0.5 at 4 GeV incident energy[1,2,3] to∿ 0.8 at our energy, a rise that is consistent with the steeper energy dependence of the unnatural parity exchanges (i.e., K, Q_A, and Q_B).

3.5 SU3 Comparisons

Using SU3 with ideal mixing and certain additional assumptions,

one obtains the prediction that the cross sections for $K^-p \to \rho^0(\Lambda,\Sigma^0)$ and $K^-p \to \omega(\Lambda,\Sigma^0)$ should be equal.[1,10] Further it is predicted that $K^-p \to \phi(\Lambda,\Sigma^0)$ and $K^-p \to \rho^0(\Lambda,\Sigma^0)$ be related as a line reversal pair: in particular if the contributing trajectories are exchange degenerate then the cross section for ϕ production should be twice that for ρ^0 production. Both predictions can be understood by comparing the duality diagrams for these reactions shown in Fig. 7. If one ignores the non-interacting top quark line, which is different for the two diagrams, it is clear that a line reversal relates them. The factor of two arises from the fact that the $\bar{p}p$ pair in Fig. 7b is an equal mixture of ρ^0 and ω.

This prediction also applies independently to the individual components of the cross section: σ_+, σ_-, and σ_0. It should be noted that the relations between these components will be different for the Λ and Σ^0 final states, however the predictions $\sigma_+(\phi) = 2\sigma_+(\rho^0)$, etc., hold for the Λ and the Σ^0 independently as well as for their sum.

Comparing the experimental cross sections with this prediction, we have already observed that the shape of the σ_+ for the ρ^0 is completely consistent with σ_+ for the ϕ. If we then integrate σ_+ over t' and correct for the $\phi \to K^-K^+$ branching fraction, we obtain a ϕ to ρ^0 ratio of 1.9 ± 0.2, in good agreement with the prediction. This agreement not only suggests that at this energy the K* and K** trajectories are approximately exchange degenerate, but also that absorption of σ_+ is either weak or equal for ϕ and ρ^0 production.

On the other hand, it is apparent from Figs. 5 and 6 that the prediction is badly broken for the unnatural parity exchange components. In fact, the ϕ to ρ^0 ratio for the total cross sections is 1.5 ± 0.2,

with the deviation from two coming entirely from σ_- and σ_0. The disagreement for unnatural exchange could be the result of exchange degeneracy breaking (for K and Q_B) or of absorption.

At lower energies, where natural parity exchange is less important, σ_+ for the ϕ is larger than, but not twice σ_+ for the ρ^0 (or the ω).[1,2,3] In addition, the Λ polarization has been measured to be non-zero in these experiments, which provides evidence that the K* and K** trajectories cannot be exactly exchange degenerate.

4.0 ρ^0 - ω Interference

4.1 General Remarks

The reaction $K^-p \to \pi^-\pi^+(\Lambda,\Sigma^0)$ should have a strong ρ^0 - ω interference effect. As discussed in the previous section, SU(3) predicts that the ρ^0 and the ω production amplitudes are equal giving maximal interference.[11] This is in contrast to the effect observed with pion-produced dipion states.[12] There, the ρ^0 amplitude is mostly π exchange, which is stronger than the ω amplitude, and their sum is not necessarily coherent. ρ - ω interference has also been seen in ρ^0 photoproduction and with e^+e^- colliding beams, where the ρ^0 and ω amplitudes should be coherent, but where the ω amplitude is smaller by a factor of three.[13] The only previous report of this effect in K^-p reactions was at very low energies where a weak signal was seen.[14]

We will assume that ρ^0 - ω interference can be described by a coherent sum of normalized Breit-Wigner amplitudes:

$$\sigma(m) \propto | f_\rho(m) + \alpha e^{i\phi} f_\omega(m) |^2$$

where the parameters α and ϕ are to be determined from the data. Theoretically, the complex coefficient of f_ω is predicted by the mass matrix formalism[15] to be

$$\alpha\, e^{i\phi} = \varepsilon \frac{A\omega}{A\rho}$$

where A_ω and A_ρ are vector meson production amplitudes. The variable ε, whose modulus squared is just the $\omega \to \pi^+\pi^-$ branching ratio, is given by

$$\varepsilon = \frac{\delta}{m_\rho - m_\omega - i\,\Gamma\rho/2}\left(\frac{\Gamma_\rho}{\Gamma_\omega}\right)^{1/2}$$

where δ measures the electromagnetic mixing of the ρ^0 and the ω. The theoretical prediction for the magnitude of δ is 2.5 MeV, and it is expected to be real.[16]

Therefore, assuming that ϕ yields the relative phase of the ρ^0 and ω amplitudes:

$$\phi = \arg(A\omega/A\rho) + \arg(\varepsilon)$$
$$\approx \arg(A\omega/A\rho) + 103^\circ.$$

The value of α, on the other hand, can be interpreted two different ways. If we assume δ = 2.5 MeV (or alternatively that $|\varepsilon|^2$ has been well measured) than α determines the ratio of $|A\omega|$ to $|A\rho|$:

$$\alpha = |\varepsilon| \frac{|A\omega|}{|A\rho|} \approx 0.13 \frac{|A\omega|}{|A\rho|}$$

If instead we assume the SU(3) prediction that $A\omega = A\rho$ is true, then α^2 can be considered to be a measurement of the $\omega \to \pi^+\pi^-$ branching ratio, $|\varepsilon|^2$. It should be noted that the assumption of complete coherence for $A\omega$ and $A\rho$ means that the measured value of α is essentially a lower limit.[14]

4.2 Results

The experimental $\pi^-\pi^+$ mass distribution in the ρ^0 region has been replotted in Fig. 8 with the $K^-\pi^+$ contamination subtracted. There is a clearly visible notch in the ρ^0 peak just above the ω

mass. We have fit these data to a coherent sum of acceptance corrected Breit-Wigners plus a possible incoherent linear background. The fitting function has been smeared by the $\pi^- \pi^+$ mass resolution, which is estimated to be $\pm$ 8 MeV. With the ρ^0 and ω parameters fixed at the values[17]

$m_\rho = 0.765$ GeV $\quad\quad \Gamma_\rho = 0.150$ GeV

$m_\omega = 0.7827$ GeV $\quad\quad \Gamma_\omega = 0.010$ GeV

the best fit to the ρ^0 line shape was obtained with a simple relativistic Breit-Wigner and no additional background. The fit extended from 0.6 to 0.92 GeV and gave a χ^2 of 31 for 29 degrees of freedom (D.F.);
it is shown by the solid curve in Fig. 8. The values of the fitted parameters and their statistical errors are $\alpha = 0.19 \pm 0.04$ and $\phi = 99^\circ \pm 10^\circ$.

To test that the interference is a significant effect, we have also performed a fit without the ω contribution. This fit is shown by the dashed curve in Fig. 8 and yielded a χ^2 of 81 for 31 D.F. The increase of 50 in χ^2 for 2 additional degrees of freedom demonstrates that the interfering ω is indeed required by the data.

We have also used a modified P-wave Breit-Wigner[18] for the ρ^0, which does not fit the high mass tail as well ($\chi^2 = 39$ for 29 D.F.). The results of this fit were $\alpha = 0.21 \pm 0.04$ and $\phi = 104^\circ \pm 10^\circ$, showing that the interference parameters are not very sensitive to the ρ^0 parameterization. Other variations that were also tried were to vary the ρ^0 and ω masses and widths within the range of previous measurements[17] and to vary the experimental mass resolution. We conclude from these studies that the additional uncertainties due

to the parameterization of the fitting function are $\pm$ 0.03 for α and $\pm 5^\circ$ for ϕ. Adding these in quadrature to the statistical errors our final results are

$\alpha = 0.19 \pm 0.05$

$\phi = 99^\circ \pm 11^\circ$.

Using the assumptions discussed above, we thus obtain the following relations between the ρ^0 and ω production amplitudes:

$\arg(A\omega/A\rho) = -4^\circ \pm 11^\circ$

$|A\omega/A\rho| = 1.5 \pm 0.4$

The phase measurement is in excellent agreement with the SU(3) prediction of equal amplitudes, while the weaker measurement of the ratio is at least consistent with the prediction. If we assume that $A\omega$ and $A\rho$ are indeed equal, then our measured value of α yields the branching ratio:

$$\frac{\Gamma(\omega \to \pi^+\pi^-)}{\Gamma(\omega \to \text{all})} = 0.035 \pm 0.018.$$

This result is larger than, but consistent with the world average[17] of 0.013 ± 0.003. Assuming that the mass mixing parameter δ is 2.5 MeV, the theoretically predicted branching ratio is 0.017.

5.0 S* Production

In the $\pi^-\pi^+$ mass spectrum shown in Fig. 8 there is also a small peak at $\sim$ 0.98 GeV, which rises above the extrapolated $\rho^0 + \omega$ fit of the previous section (dotted line). We interpret this peak as evidence for the production of the S*(993) meson. Previous evidence for the existence of this state comes from investigations of $\pi\pi$ scattering in $\pi^\pm p$ experiments.[19,20] In these studies the S-wave elasticity is observed to drop sharply at $\bar{K}K$ threshold, indicating the presence of a $\pi\pi$ state which couples strongly to the $\bar{K}K$

channel. A threshold enhancement is also observed in the $\pi\pi \to \bar{K}K$ data. In the reaction $K^-p \to \pi^-\pi^+(\Lambda,\Sigma^0)$, one can study the reverse process $\bar{K}K \to \pi\pi$ via K exchange. Here it is possible to have a $\bar{K}K$ system below threshold, thus making it feasible to observe the S* state over a wider mass range.

In order to check that the effect we see is really the S*, we have computed the expected $\pi\pi$ mass dependence from the K matrix parameters determined in previous experiments. The data is replotted in Fig. 9 with the ρ^0 tail as well as the $K^-\pi^+$ contamination subtracted. The three curves correspond to the S* parameters shown in Table I.[‡] The solid and dashed curves give the best χ^2 (7 for 8 D.F.), but all three curves are clearly consistent with the peak in the data.

Having observed the S* in the $\pi^-\pi^+$ mass spectrum, it is interesting to check if a K^-K^+ threshold enhancement exists in the reaction $K^-p \to K^-K^+(\Lambda,\Sigma^0)$. Although the couplings of the S* favor the $\bar{K}K \to \bar{K}K$ channel over $\bar{K}K \to \pi\pi$, there is a factor of q, the final state CMS momentum, in the cross section, which reduces the expected K^-K^+ effect to less than half of the $\pi^-\pi^+$ effect. The few events that one might expect to see are swamped by the tails of the large ϕ peak, as can be seen in Fig. 3b.

I would like to thank my former colleagues at SLAC for their hospitality while this talk was being prepared.

---

‡ The complex couplings are defined as follows: The residues at the pole are $R_{ij} = \lim_{E \to E_o} (E_o - E)\, T_{ij}$; they satisfy $R_{11}R_{22} - R_{12}^2 = 0$. We may thus take $g_i = + \sqrt{R_{ii}}$ as the dimensionless couplings.

REFERENCES

1. M. Aguilar-Benitez, S.U. Chung, R.L. Eisner, and N.P. Samios, Phys. Rev. D6, 29 (1972); R.D. Field, R.L. Eisner, and M. Aguilar-Benitez, Phys. Rev. D6, 1863 (1972).
2. A. Rougé et al., Nucl. Phys. B44, 365 (1972).
3. A.J. de Groot et al., Nucl. Phys. B74, 77 (1974).
4. G.W. Brandenburg, R.K. Carnegie, R.J. Cashmore, M. Davier, T.A. Lasinski, D.W.G.S. Leith, J.A.J. Matthews, P. Walden, and S. Williams, to be published.
5. R.K. Carnegie et al., to be published.
6. H.H. Williams, A. Kilert, and D.W.G.S. Leith, Nucl. Instrum. Methods 105, 483 (1972).
7. P.K. Williams and V. Hagopian, Proc. Int. Conf. on $\pi\pi$ Scattering, American Institute of Physics, New York, 1973.
8. G.A. Ringland and R.L. Thews, Phys. Rev. 170, 1569 (1968); J.P. Ader, M. Capdeville, G. Cohen-Tannoudji, and Ph. Salin, Nuovo Cimento 56A, 952 (1968).
9. M. Ross, F.S. Henyey, and G.L. Kane, Nucl. Phys. B23, 269 (1970).
10. H.J. Lipkin, Nucl. Phys. B7, 321 (1968).
11. A.S. Goldhaber, G.C. Fox, and C. Quigg, Phys. Lett. 30B, 249 (1969).
12. B.N. Ratcliff et al., Phys. Lett. 38B, 346 (1972); S.L. Kramer et al., Phys. Rev. Lett. 33, 505 (1974); P. Estabrooks et al., Nucl. Phys. B81, 70.
13. R. Marshall, Proc. Int. Conf. on Meson Resonances and Related Phenomena, P. 101, Bologna, 1971.
14. S.M. Flatté, Phys. Rev. D1, 1 (1970).

15. G. Goldhaber, Experimental Meson Spectroscopy, p. 59, Columbia University Press, New York, 1970.

16. S. Coleman and S.L. Glashow, Phys. Rev. 134B, 671 (1964).

17. Particle Data Group, Phys. Lett. 50B, 1 (1974).

18. J. Pisut and M. Roos, Nucl. Phys. B6, 325 (1968).

19. B. Hyams et al., Nucl. Phys. B64, 134 (1973).

20. S.D. Protopopescu et al., Phys. Rev. D7, 1279 (1973).

Table I: Resonance parameters associated with the curves shown in Fig. 9

Curve	Pole (MeV)	$g_{\pi\pi}$	g_K	χ^2 (9 bins)
C-M (Ochs)[19]	$(1006-i\ 15)_{II}$	$0.28e^{i76^\circ}$	$0.55e^{-i29^\circ}$	7.4
LBL (Casel)[20]	$(997-i\ 27)_{II}$	$0.30e^{-i84^\circ}$	$0.47e^{i11^\circ}$	16.0
	$(930-i\ 18)_{III}$	$0.19e^{-i65^\circ}$	$0.63e^{i18^\circ}$	
LBL (const.K)[20]	$(1002-i\ 33)_{II}$	$0.35e^{-i89^\circ}$	$0.73e^{-i31^\circ}$	7.0

FIGURE CAPTIONS

1. Experimental layout.
2. Recoil missing mass spectrum from (a) ϕ mesons and (b) ρ^0 mesons.
3. K^-K^+ mass spectrum (a) entire range with K^+ identified (b) ϕ region with positive particle not a π^+.
4. $\pi^-\pi^+$ mass spectrum. Dotted curve is estimated $K^-\pi^+$ contamination.
5. Differential cross sections and exchange parity components for ϕ production in (a) t-channel and (b) s-channel helicity frames.
6. Differential cross sections and exchange parity components for ρ^0 production in the t-channel helicity frame.
7. Quark duality diagrams for (a) $K^-p \to (\Lambda,\Sigma^0)\phi$ and (b) $K^-p \to (\Lambda,\Sigma^0)(\rho^0,\omega)$.
8. $\pi^-\pi^+$ mass spectrum in ρ^0 region with $K^-\pi^+$ contamination subtracted. See text for description of curves.
9. $\pi^-\pi^+$ mass spectrum in S* region with $K^-\pi^+$ contamination and ρ^0 tail subtracted. See text for description of curves.

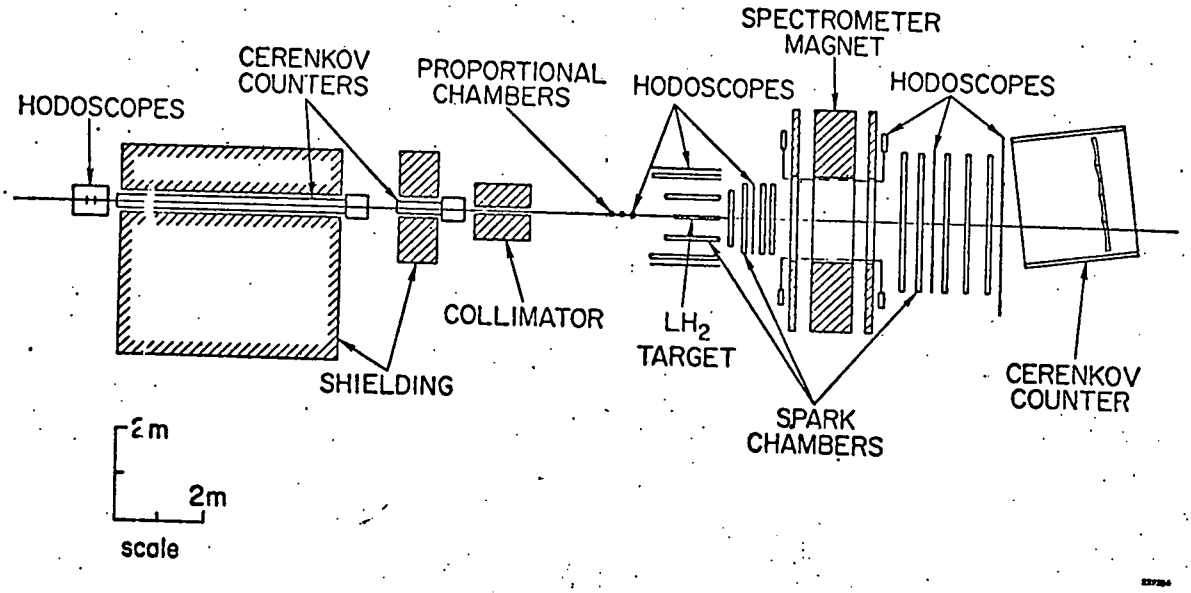

Figure 1

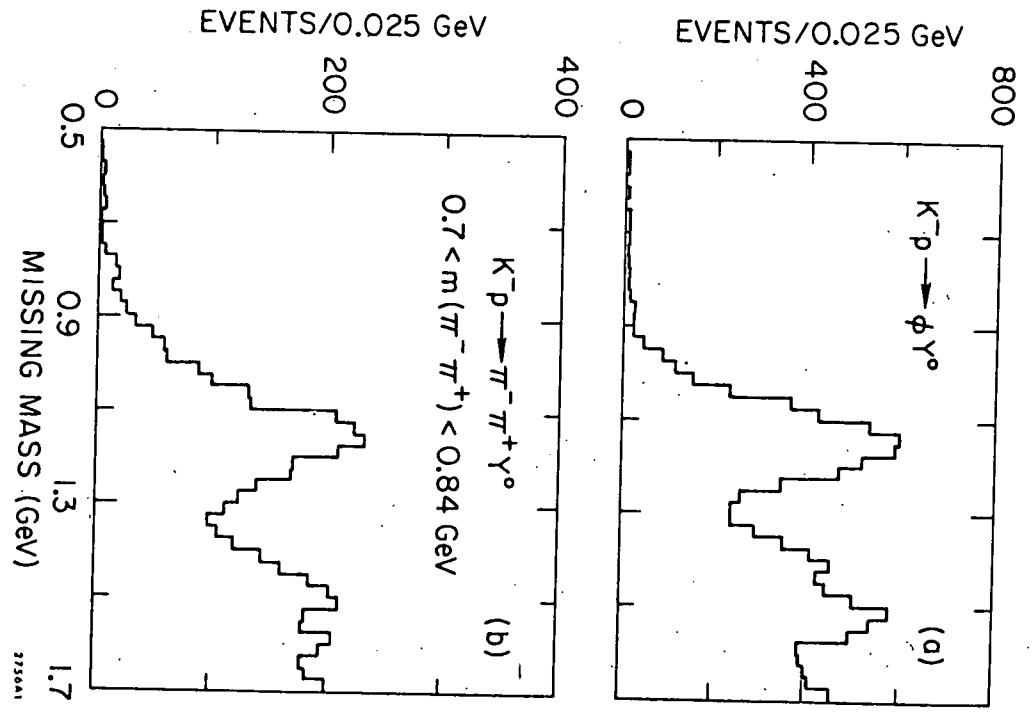

Figure 2

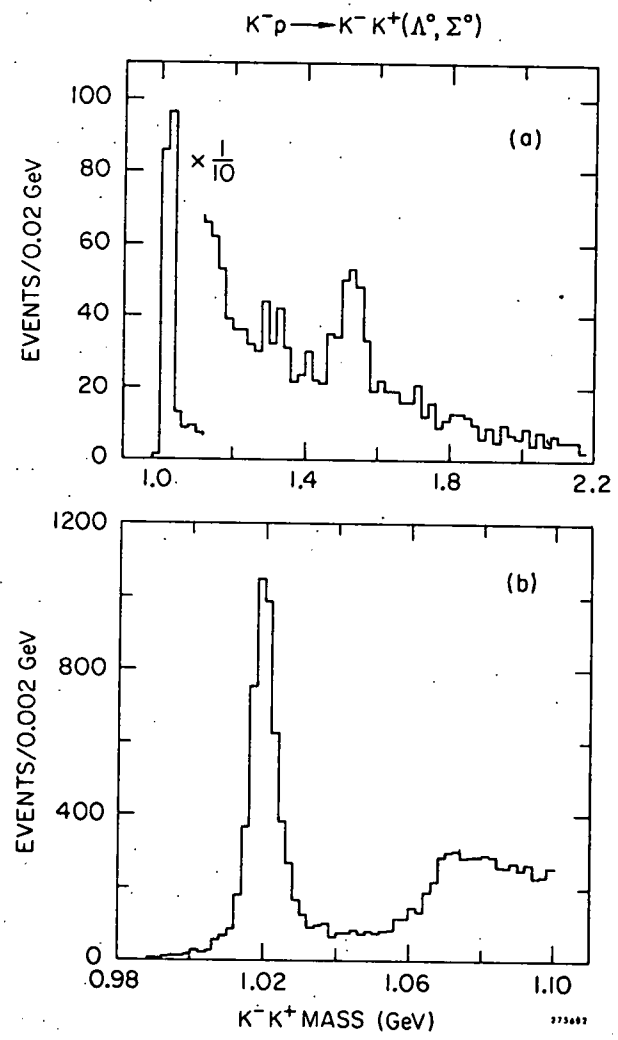

Figure 3

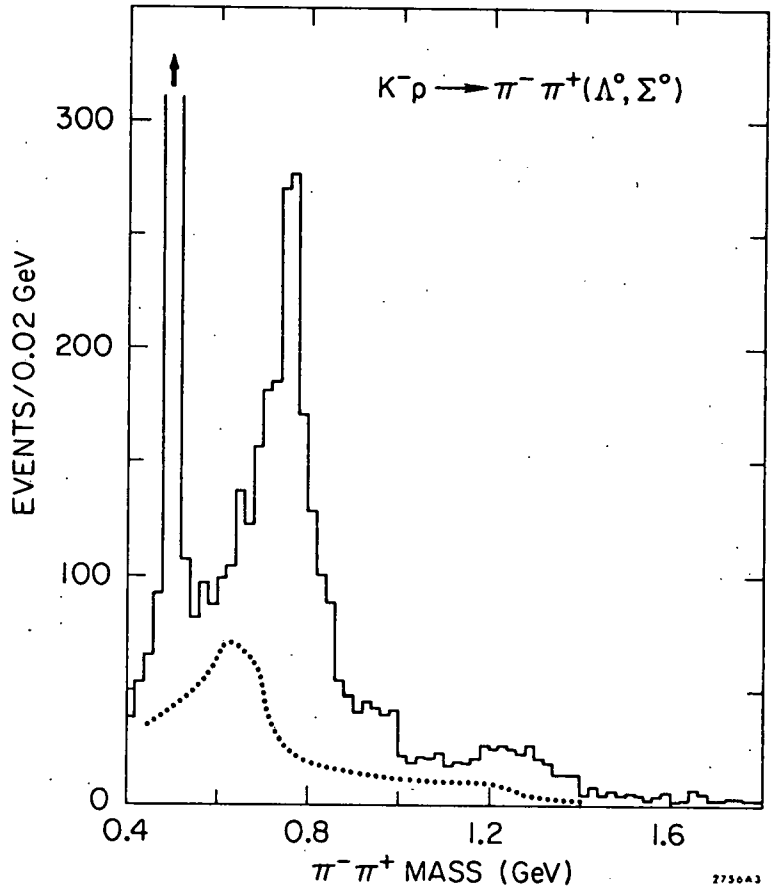

Figure 4

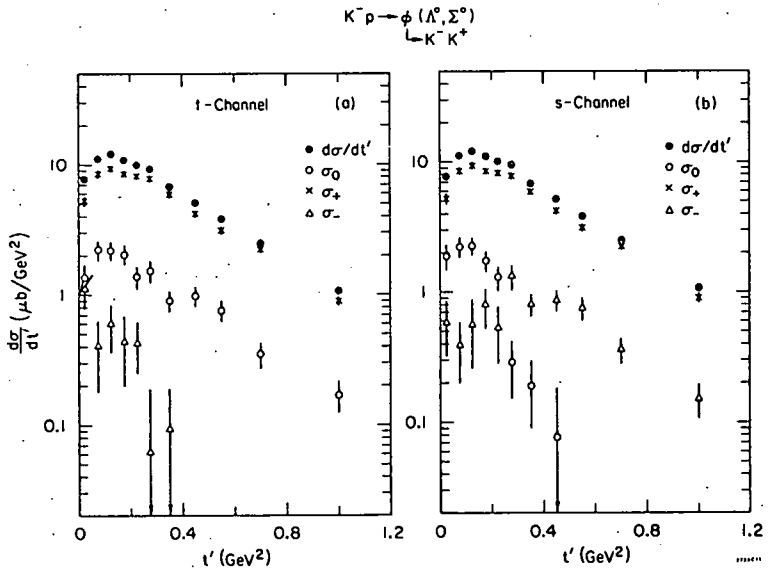

Figure 5

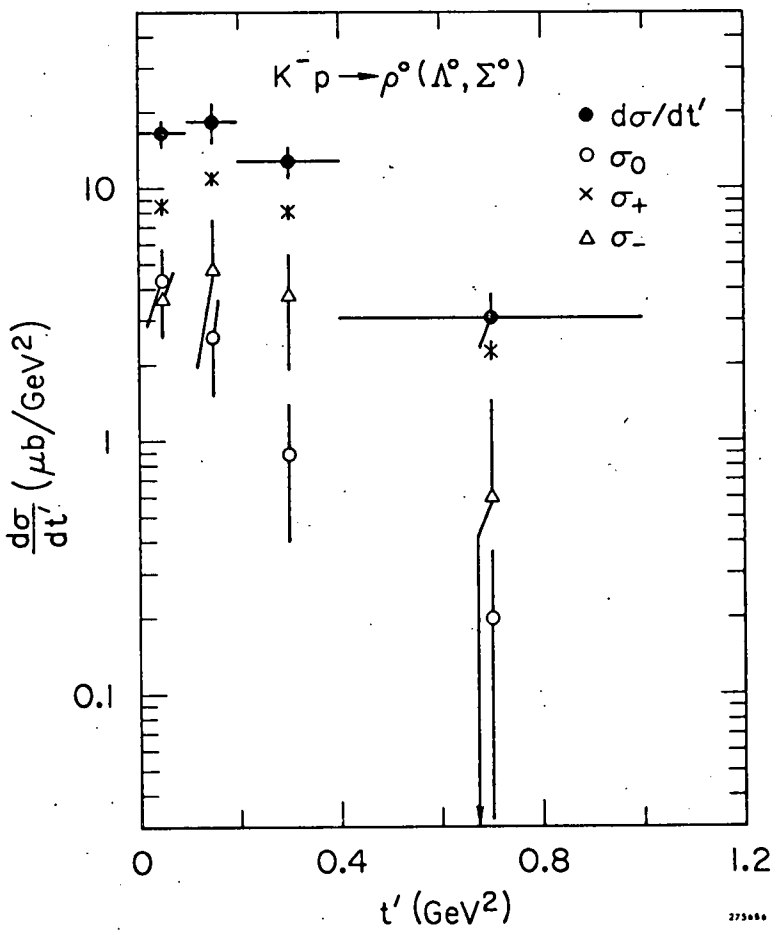

Figure 6

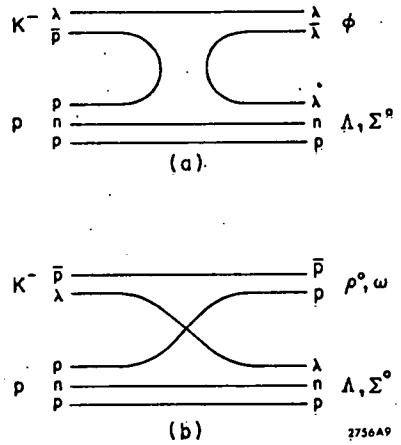

Figure 7

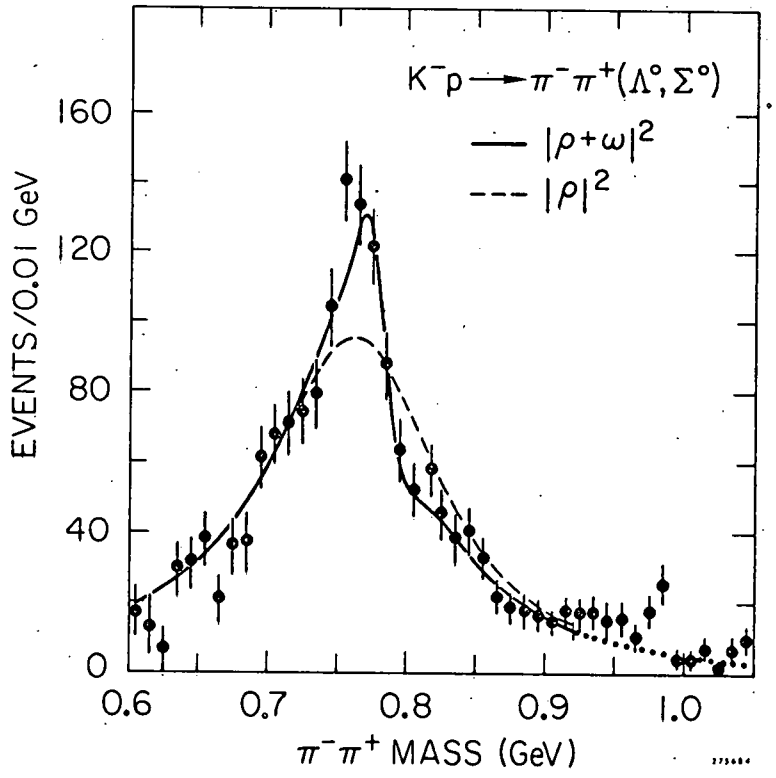

Figure 8

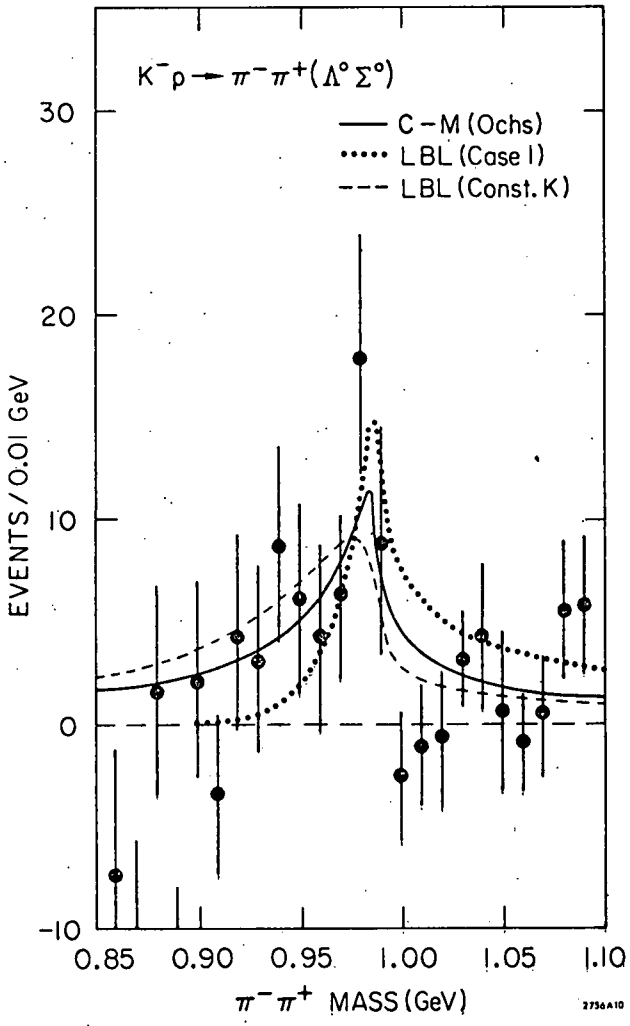
$K^-p \to \pi^-\pi^+(\Lambda^\circ\Sigma^\circ)$
C – M (Ochs)
LBL (Case I)
LBL (Const. K)
EVENTS / 0.01 GeV
30
20
10
0
-10
0.85
0.90
0.95
1.00
1.05
1.10
$\pi^-\pi^+$ MASS (GeV)
2736A10

Figure 9